High-Gain Disturbance Observer for Robust Trajectory Tracking of Quadrotors

Mohammadreza Izadi, Reza Faieghi

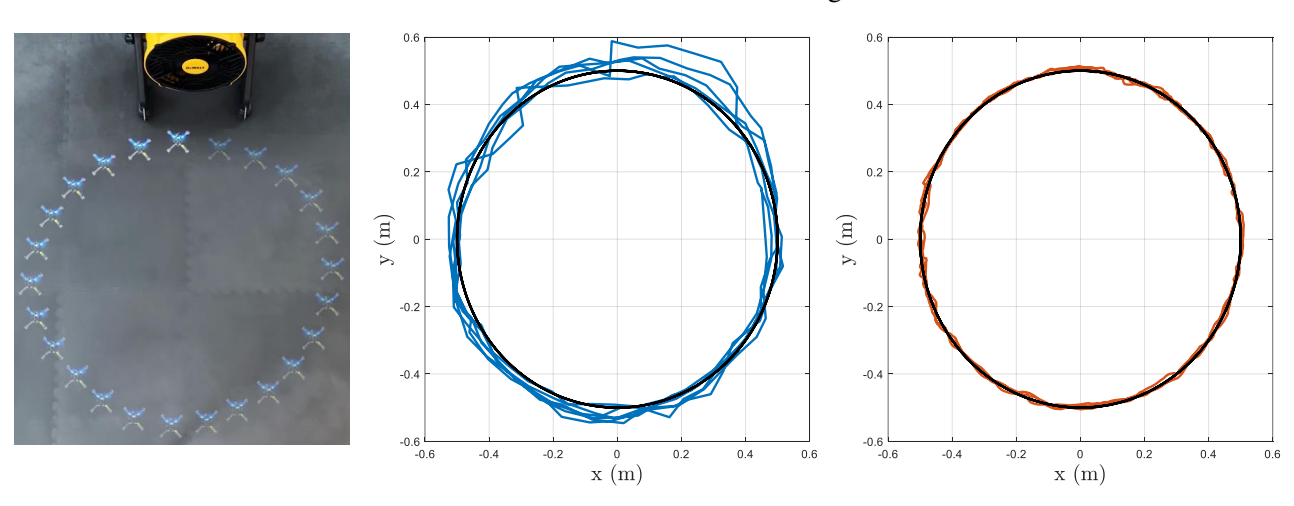


Fig. 1: The boost in robustness by adding a high-gain disturbance observer (HGDO) to the flight controller. Left: Laboratory experiment setup where a nano quadrotor (Crazyflie 2.1) is repetitively completing a circular path. A disturbance is generated by an external fan. Middle: The vehicle trajectory with a fine-tuned sliding mode control (SMC) as a typical robust controller. Right: The vehicle trajectory with the same SMC but augmented with HGDO. Both the accuracy and precision of the trajectory tracking are significantly improved.

Abstract—This paper presents a simple method to boost the robustness of quadrotors in trajectory tracking. The presented method features a high-gain disturbance observer (HGDO) that provides disturbance estimates in real-time. The estimates are then used in a trajectory control law to compensate for disturbance effects. We present theoretical convergence results showing that the proposed HGDO can quickly converge to an adjustable neighborhood of actual disturbance values. We will then integrate the disturbance estimates with a typical robust trajectory controller, namely sliding mode control (SMC), and present Lyapunov stability analysis to establish the boundedness of trajectory tracking errors. However, our stability analysis can be easily extended to other Lyapunov-based controllers to develop different HGDO-based controllers with formal stability guarantees. We evaluate the proposed HGDO-based control method using both simulation and laboratory experiments in various scenarios and in the presence of external disturbances. Our results indicate that the addition of HGDO to a quadrotor trajectory controller can significantly improve the accuracy and precision of trajectory tracking in the presence of external disturbances.

I. INTRODUCTION

QUADROTORS are susceptible to various external disturbances. Examples include wind gusts [1], airflow distortion in the vicinity of surfaces [2], and wake turbulence [3]. Such disturbances are often unmodelled or are difficult to

The authors are with the Autonomous Vehicles Laboratory, Department of Aerospace Engineering, Toronto Metropolitan University, Toronto, Canada {mizadi,reza.faieghi}@torontomu.ca. This work was supported by the Natural Sciences and Engineering Research Council (NSERC) of Canada.

measure, posing formidable challenges to accurately control the vehicle trajectory.

Various control approaches are studied for robust trajectory tracking of quadrotors in the presence of disturbances. Examples include model predictive control [4]–[6], sliding mode control (SMC) [7]–[9], adaptive control [10]–[12], neural networks [13]–[15], and reinforcement learning [16]–[18]. Ample evidence shows these methods can handle disturbances to certain extents.

However, a higher degree of robustness can be achieved if an estimate of disturbance is available (as is the case with our results in Fig. 1). Numerous studies have explored the design of disturbance observers (DOs) for quadrotors; see, for example, [19]–[24]. The DO estimates external disturbances and provides the estimated disturbance to the controller. The controller incorporates this information in the control law to reject disturbances more effectively and attain higher robustness [25].

DO design methods for quadrotors root back to nonlinear observer design methods, especially sliding mode and adaptive observers [26]. The stability and convergence characteristics of such DOs can be studied using Lyapunov stability analysis. Numerical and laboratory experiments have shown that such DOs can successfully handle disturbances, and even enable aggressive maneuvers [27] and fault tolerance [28]. However, sliding mode and adaptive DOs often lead to complex structures that can become computationally prohibitive for implementation on flight controllers. They also involve several tuning parameters which require an involved tuning

process to ensure a fast convergence rate.

One category of nonlinear observers that, in contrast to sliding mode and adaptive observers, are simple and fast is high-gain observers (HGOs) [29]. As its name suggests, HGO relies on the idea of applying a high gain to quickly recover the state estimates. HGOs present several desirable properties. First, they are relatively simple to design and implement since the observer is a copy of the model of the system with a gain whose expression is explicitly given. Second, the observer tuning is realized simply through the choice of a single scalar design parameter. Finally, they can provide global or semi-global stability results for a large class of systems. Such appealing properties; however, come at a cost. Conventional HGOs suffer from measurement noise amplification; however, this problem is alleviated by recent designs [30], [31].

Given the advantages of HGOs, their applications for disturbance estimation are also explored, giving rise to highgain disturbance observers (HGDOs) [32]. However, the application of HGDOs for quadrotors has not been thoroughly studied. The papers that we were able to find on this topic either presented a limited simulation study or focused on only attitude control [33]–[36]. Another related work is [37] which does not design HGDO, but rather an HGO for quadrotor state estimation, as an alternative to the extended Kalman filter.

In light of the above discussion, our objective here is to design HGDO for six degrees-of-freedom trajectory control of quadrotors. The main contribution of this paper is that it presents a new HGDO for the attitude and position control of quadrotors. To handle measurement noise effects, we base our approach on the idea of using auxiliary variables presented in [31]. This HGDO uses a simple formulation which additionally facilitates the mathematical treatments for control design and stability analysis. As our focus is on the HGDO design and its integration with existing controllers, we use a typical robust controller, namely sliding mode control (SMC). We present Lyapunov stability analysis to establish the boundedness of tracking errors and disturbance estimations. The SMC can be easily replaced by another Lyapunov-based controller, and a similar stability analysis can be derived for the alternative controller. Overall, our intention is not a major overhaul in the quadrotor flight control, but rather to introduce a simple, easy-to-tune, and computationally efficient module that can be added to a flight controller and boost trajectory tracking robustness against external disturbances. As our experiments will demonstrate, our proposed HGDO presents fast convergence performance and can significantly improve vehicle accuracy and precision in trajectory tracking tasks.

II. QUADROTOR MODELING

The details of the quadrotor model are explained in various references such as [38]. Here, we attempt to write the quadrotor translation and rotational dynamics in second-order controllability canonical forms which will become

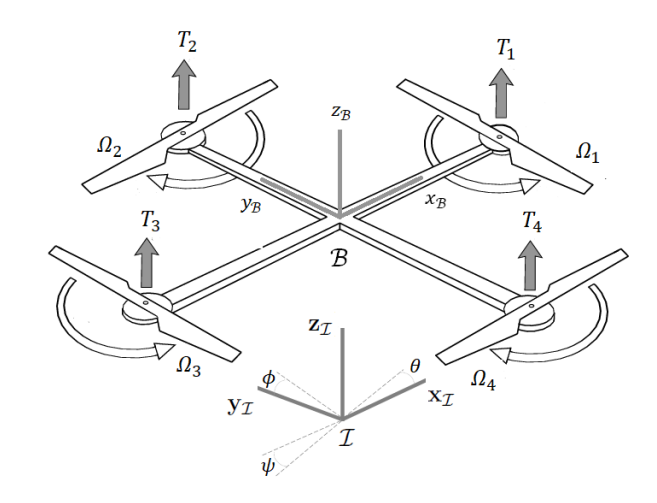


Fig. 2: Quadrotor model and coordinate frames

useful in our developments. The problem statement will follow.

Let us begin by setting $\mathcal{I} = \{\mathbf{x}_{\mathcal{I}}, \mathbf{y}_{\mathcal{I}}, \mathbf{z}_{\mathcal{I}}\}$ as an Earth-fixed inertial coordinates frame, and $\mathcal{B} = \{\mathbf{x}_{\mathcal{B}}, \mathbf{y}_{\mathcal{B}}, \mathbf{z}_{\mathcal{B}}\}$ as the body-fixed coordinates frame whose origin coincides with the center of mass of the vehicle (Figure 2). We assume that the quadrotor body is rigid and symmetric, with arms aligned to $\mathbf{x}_{\mathcal{B}}$ and $\mathbf{y}_{\mathcal{B}}$. The length of each arm is l, and the mass of the vehicle is m. Also, the inertia matrix is \mathbf{J} which is diagonal $\mathbf{J} = \mathrm{diag}\left(J_x, J_y, J_z\right)$ due to the symmetry of the vehicle.

We denote the position of the vehicle in \mathcal{I} by $\boldsymbol{\xi} = [x,y,z]^T$. For the vehicle attitude, we use $\boldsymbol{\eta} = [\phi,\theta,\psi]^T$, where $-\pi < \phi \leq \pi$, $-\frac{\pi}{2} \leq \theta \leq \frac{\pi}{2}$, and $-\pi < \psi \leq \pi$ are the Euler angles representing pitch, roll, and yaw in the yaw-pitch-roll sequence. Also, with the above Euler angle configuration, the rotation matrix from \mathcal{B} to \mathcal{I} takes the following form

$$\mathbf{R} = \begin{bmatrix} c\theta c\psi & s\phi s\theta c\psi - c\phi s\psi & c\phi s\theta c\psi + s\phi s\psi \\ c\theta s\psi & s\phi s\theta s\psi + c\phi c\psi & c\phi s\theta s\psi - s\phi c\psi \\ -s\theta & s\phi c\theta & c\phi c\theta \end{bmatrix}, (1)$$

where c and s stand for cosine and sine functions. Also, if $\boldsymbol{\omega} = [p,q,r]^T$ represent the angular velocity vector, then according to the Euler kinematical equation, we have $\dot{\boldsymbol{\eta}} = \mathbf{H}(\boldsymbol{\eta}) \boldsymbol{\omega}^{\mathcal{B}}$, where the superscript \mathcal{B} indicates that the vector components are expressed in \mathcal{B} and

$$\mathbf{H}(\boldsymbol{\eta}) = \begin{bmatrix} 1 & \sin\phi \tan\theta & \cos\phi \tan\theta \\ 0 & \cos\phi & -\sin\phi \\ 0 & \sin\phi/\cos\theta & \cos\phi/\cos\theta \end{bmatrix}. \tag{2}$$

Each of the vehicle's rotors produces a thrust T_i , $i = \{1, 2, 3, 4\}$ in the direction of $\mathbf{z}_{\mathcal{B}}$. T_i s are usually approximated by $k_T\Omega_i^2$ where Ω_i is the angular velocity of i-th rotor, and k_T is a coefficient. The rotor angular velocities on the $\mathbf{x}_{\mathcal{B}}$ and $\mathbf{y}_{\mathcal{B}}$ axes have opposite signs $(\Omega_{1,3} > 0, \Omega_{2,4} < 0)$ to counterbalance the reaction torque induced by the rotors and to control ψ . Let \mathbf{f}_A and $\boldsymbol{\tau}_A$ be the aerodynamic force

and torque vectors produced by T_i s. Then, we can express them in \mathcal{B} as follows

$$\mathbf{f}_{A}^{\mathcal{B}} = \begin{bmatrix} 0 \\ 0 \\ T \end{bmatrix}, \text{ and } \boldsymbol{\tau}_{A}^{\mathcal{B}} = \begin{bmatrix} lk_{T} \left(\Omega_{4}^{2} - \Omega_{2}^{2}\right) \\ lk_{T} \left(\Omega_{3}^{2} - \Omega_{1}^{2}\right) \\ lk_{Q} \left(\Omega_{1}^{2} - \Omega_{2}^{2} + \Omega_{3}^{2} - \Omega_{4}^{2}\right) \end{bmatrix}$$

where $T=k_T\sum_{i=1}^4\Omega_i^2$ is the total thrust, and k_Q is a coefficient. In addition, we assume that there exist two unknown disturbance vectors $\mathbf{d}_{\boldsymbol{\xi}} = [d_x, d_y, d_z]^T$ and $\mathbf{d}_{\boldsymbol{\eta}} =$ $[d_{\phi}, d_{\theta}, d_{\psi}]^T$.

Applying Newton's law of motion, the translational dynamics of the vehicle take the following form

$$\ddot{\boldsymbol{\xi}} = -\mathbf{g} + \frac{1}{m} \left(\mathbf{f}_A^{\mathcal{I}} + \mathbf{d}_{\boldsymbol{\xi}}^{\mathcal{I}} \right), \tag{4}$$

where $\mathbf{f}_A^{\mathcal{I}} = \mathbf{R}\mathbf{f}_A^{\mathcal{B}}$, $\mathbf{d}_{\boldsymbol{\xi}}^{\mathcal{I}} = \mathbf{R}\mathbf{d}_{\boldsymbol{\xi}}^{\mathcal{B}}$ and $\mathbf{g} = \begin{bmatrix} 0 \ 0 \ g \end{bmatrix}^T$ is the gravity vector with g set to $9.81m/s^2$. Using Euler's rotation theorem, the rotational dynamics of the vehicle take the following form

$$\dot{\boldsymbol{\omega}}^{\mathcal{B}} = \mathbf{J}^{-1} \left(\boldsymbol{\omega}_{\times}^{\mathcal{B}} \mathbf{J} \boldsymbol{\omega}^{\mathcal{B}} + \boldsymbol{\tau}_{A}^{\mathcal{B}} + \mathbf{d}_{\boldsymbol{\xi}}^{\mathcal{B}} \right), \text{ and } \dot{\boldsymbol{\eta}} = \mathbf{H} \left(\dot{\boldsymbol{\eta}} \right) \boldsymbol{\omega}^{\mathcal{B}},$$
(5)

where the index \times indicates the cross-product matrix.

We can now use (4) and (5) to write the quadrotor dynamics as a set of second-order nonlinear systems in controllability canonical forms. However, due to the particular structure of (5), the equations will become complicated, and this will lead to complex DO and control laws. If ϕ and θ are small, **H** can be greatly simplified such that $\dot{\eta} \approx \omega$. As such, we can express the translational and rotational dynamics as follows

$$\begin{cases}
\dot{\mathbf{x}}_{1} = \mathbf{x}_{2}, \\
\dot{\mathbf{x}}_{2} = -\mathbf{g} + \mathbf{u}_{1} + \mathbf{d}_{1}, \\
\dot{\mathbf{x}}_{3} = \mathbf{x}_{4}, \\
\dot{\mathbf{x}}_{4} = \mathbf{f}_{2}(\mathbf{x}_{4}) + \mathbf{u}_{2} + \mathbf{d}_{2},
\end{cases}$$
(6)

where $\mathbf{x}_1 = \boldsymbol{\xi}, \ \mathbf{x}_2 = \dot{\boldsymbol{\xi}}, \ \mathbf{x}_3 = \boldsymbol{\eta}, \ \mathbf{x}_4 = \dot{\boldsymbol{\eta}}, \ \mathbf{d_1} = \frac{\mathbf{d_{\boldsymbol{\xi}}}}{m}, \ \mathbf{d_2} = \mathbf{J}^{-1}\mathbf{d_{\boldsymbol{\eta}}}, \ \mathbf{u}_1 = \frac{1}{m}\mathbf{Rf}_A^{\mathcal{B}}, \ \mathbf{u}_2 = \mathbf{J}^{-1}\boldsymbol{\tau}_A^{\mathcal{B}}$ and

$$\mathbf{f}_{2}(\mathbf{x}_{4}) = \begin{bmatrix} \frac{I_{y} - I_{z}}{I_{x}} \dot{\theta} \dot{\psi} \\ \frac{I_{z} - I_{x}}{I_{y}} \dot{\phi} \dot{\psi} \\ \frac{I_{x} - I_{y}}{I_{z}} \dot{\phi} \dot{\theta} \end{bmatrix}.$$

Note that since we assume ϕ and θ to be small, our developments are not valid for aggressive maneuvers with high pitch or roll. However, the above approximation is commonly used in the literature, and as it will turn out in our experiments, such an approximation tends to work fine for a variety of common maneuvers.

Our first objective is to design an HGDO that can estimate d_1 and d_2 . Our second objective is to use the disturbance estimates and design control laws \mathbf{u}_1 and \mathbf{u}_2 such that the vehicle can follow a desired trajectory $(\mathbf{x}_{1d}^T, \mathbf{x}_{3d}^T)^T$ in the presence of unknown disturbances. Once \mathbf{u}_1 and \mathbf{u}_2 are determined, $\mathbf{f}_A^{\mathcal{B}}$ and $\boldsymbol{\tau}_A^{\mathcal{B}}$ can be determined. Then, Ω_i can be calculated using the following expression

them in
$$\mathcal{B}$$
 as follows
$$\mathbf{f}_{A}^{\mathcal{B}} = \begin{bmatrix} 0 \\ 0 \\ T \end{bmatrix}, \text{ and } \boldsymbol{\tau}_{A}^{\mathcal{B}} = \begin{bmatrix} lk_{T} \left(\Omega_{4}^{2} - \Omega_{2}^{2}\right) \\ lk_{T} \left(\Omega_{3}^{2} - \Omega_{1}^{2}\right) \\ lk_{Q} \left(\Omega_{1}^{2} - \Omega_{2}^{2} + \Omega_{3}^{2} - \Omega_{4}^{2}\right) \end{bmatrix}, \qquad \begin{bmatrix} \Omega_{1}^{2} \\ \Omega_{2}^{2} \\ \Omega_{3}^{2} \\ \Omega_{4}^{2} \end{bmatrix} = \begin{bmatrix} \frac{1}{4k_{T}} & 0 & -\frac{1}{2lk_{T}} & -\frac{1}{4k_{Q}} \\ \frac{1}{4k_{T}} & \frac{1}{2lk_{T}} & 0 & \frac{1}{4k_{Q}} \\ \frac{1}{4k_{T}} & 0 & \frac{1}{2lk_{T}} & -\frac{1}{4k_{Q}} \\ \frac{1}{4k_{T}} & -\frac{1}{2lk_{T}} & 0 & \frac{1}{4k_{Q}} \end{bmatrix} \begin{bmatrix} T \\ \boldsymbol{\tau}_{A}^{B} \end{bmatrix}.$$

We assume that the disturbance terms d_1 and d_2 and their derivatives are bounded. Let us denote the j-th component of \mathbf{d}_i , $i = \{1, 2\}$ by d_i^{\jmath} . Then,

$$\left\|\dot{d}_i^j\right\| \le \delta_i^j,\tag{8}$$

where δ_i^j s denote unknown but finite positive constants and $\|\cdot\|$ is the \mathcal{L}_1 norm defined as $\|\chi(t)\| = \int_0^t \chi(\alpha) d\alpha$. The disturbance terms can generally include unknown external disturbances, gyroscopic effects of rotors, or aerodynamic effects such as drag. The models for gyroscopic effects or drag exist in the literature [39] and one can include them in (4) and (5) to have a more elaborated model. However, these effects can be combined into disturbance terms in each axes, and HGDO can estimate their amplitudes. Therefore, one advantage of using HGDO is reducing the need for complex models.

III. HIGH-GAIN DISTURBANCE OBSERVER DESIGN

Our objective in this section is to design an HGDO to estimate d_1 and d_2 . Let d_1 and d_2 be the estimated values of d_1 and d_2 . The basic idea behind HGDO is to construct an observer of the following form

$$\begin{cases}
\dot{\hat{\mathbf{d}}}_1 = \frac{1}{\varepsilon_1} \left(\mathbf{d}_1 - \hat{\mathbf{d}}_1 \right), \\
\dot{\hat{\mathbf{d}}}_2 = \frac{1}{\varepsilon_2} \left(\mathbf{d}_2 - \hat{\mathbf{d}}_2 \right),
\end{cases} (9)$$

where $\frac{1}{\varepsilon_1}$ and $\frac{1}{\varepsilon_2}$ are the observer gains. Each equation in (9) constitutes a first-order filter of the form $\frac{1}{\varepsilon_i s+1}$. By choosing small positive values for ε_i , the settling time of the filter becomes small, and therefore \mathbf{d}_i quickly converges to \mathbf{d}_i .

Note that d_i s are unknown; however, from (6), they can be expressed as follows

$$\begin{cases}
\mathbf{d}_1 = \dot{\mathbf{x}}_2 + \mathbf{g} - \mathbf{u}_1, \\
\mathbf{d}_2 = \dot{\mathbf{x}}_4 - \mathbf{f}_2(\mathbf{x}_4) - \mathbf{u}_2.
\end{cases} (10)$$

Therefore, one can suggest the following HGDO structure for quadrotor

$$\begin{cases}
\dot{\hat{\mathbf{d}}}_1 = \frac{1}{\varepsilon_1} \left(\dot{\mathbf{x}}_2 + \mathbf{g} - \mathbf{u}_1 - \hat{\mathbf{d}}_1 \right), \\
\dot{\hat{\mathbf{d}}}_2 = \frac{1}{\varepsilon_2} \left(\dot{\mathbf{x}}_4 - \mathbf{f}_2(\mathbf{x}_4) - \mathbf{u}_2 - \hat{\mathbf{d}}_2 \right).
\end{cases} (11)$$

The drawback of (11) is the inclusion of derivatives of system states which amplifies the effect of measurement noise. Inspired by [31], we propose an HGDO using auxiliary varibles

$$\gamma_1 = \hat{\mathbf{d}}_1 - \frac{\mathbf{x_2}}{\varepsilon_1}$$
, and $\gamma_2 = \hat{\mathbf{d}}_2 - \frac{\mathbf{x_4}}{\varepsilon_2}$, (12)

with dynamics given as follows

$$\begin{cases}
\dot{\boldsymbol{\gamma}}_{1} = -\frac{1}{\varepsilon_{1}} \left(\boldsymbol{\gamma}_{1} + \frac{\mathbf{x}_{2}}{\varepsilon_{1}} \right) + \frac{1}{\varepsilon_{1}} \left(\mathbf{g}^{\mathcal{I}} - \mathbf{u}_{1} \right), \\
\dot{\boldsymbol{\gamma}}_{2} = -\frac{1}{\varepsilon_{2}} \left(\boldsymbol{\gamma}_{2} + \frac{\mathbf{x}_{4}}{\varepsilon_{2}} \right) + \frac{1}{\varepsilon_{2}} \left(-\mathbf{f}_{2}(\mathbf{x}_{4}) - \mathbf{u}_{2} \right).
\end{cases} (13)$$

To establish the convergence results for the observer, let us define the disturbance estimation error as $\tilde{\mathbf{d}}_i = \mathbf{d}_i - \hat{\mathbf{d}}_i$. Taking the derivative of $\tilde{\mathbf{d}}_i$ and using (12) result in

$$\dot{\mathbf{\dot{d}}}_1 = \dot{\mathbf{d}}_1 - \left(\dot{\boldsymbol{\gamma}}_1 + \frac{\dot{\mathbf{x}}_2}{\varepsilon_1}\right), \ \dot{\mathbf{\dot{d}}}_2 = \dot{\mathbf{d}}_2 - \left(\dot{\boldsymbol{\gamma}}_2 + \frac{\dot{\mathbf{x}}_4}{\varepsilon_2}\right).$$
 (14)

Substituting (13) in (14) leads to

$$\dot{\tilde{\mathbf{d}}}_i = -\frac{1}{\varepsilon_i} \tilde{\mathbf{d}}_i + \dot{\mathbf{d}}_i. \tag{15}$$

The above differential equations can be solved by multiplying both sides with $e^{\frac{1}{arepsilon_i}t}$ and integrating over [0,t] which yield

$$\tilde{\mathbf{d}}_{i}(t) = \tilde{\mathbf{d}}_{i}(0) e^{-\frac{1}{\varepsilon_{i}}t} + \int_{0}^{t} e^{-\frac{1}{\varepsilon_{i}}(t-\alpha)} \dot{\mathbf{d}}_{i}(\alpha) d\alpha.$$
 (16)

Writing (16) in a component-wise form and applying the absolute value operator $|\cdot|$ to both sides lead to

$$\left| \tilde{d}_{i}^{j}(t) \right| \leq \left| \tilde{d}_{i}^{j}(0) e^{-\frac{1}{\varepsilon_{i}} t} \right| + \left| \int_{0}^{t} e^{-\frac{1}{\varepsilon_{i}} (t - \alpha)} \dot{d}_{i}^{j}(\alpha) d\alpha \right|. \tag{17}$$

According to Holder's inequality [31], $\left| \int_0^t \chi\left(\tau\right) d\tau \right| \leq \int_0^t \left| \chi\left(\tau\right) \right| d\tau$. Therefore,

$$\left| \tilde{d}_{i}^{j}(t) \right| \leq \left| \tilde{d}_{i}^{j}(0) e^{-\frac{1}{\varepsilon_{i}}t} \right| + \int_{0}^{t} \left| e^{-\frac{1}{\varepsilon_{i}}(t-\alpha)} \dot{d}_{i}^{j}(\alpha) \right| d\alpha. \tag{18}$$

By integrating (18) over [0, t], we get

$$\int_{0}^{t} \left| \tilde{d}_{i}^{j} \left(\alpha \right) \right| d\alpha \leq \int_{0}^{t} \left| \tilde{d}_{i}^{j} \left(0 \right) e^{-\frac{1}{\varepsilon_{i}} \alpha} \right| d\alpha
+ \int_{0}^{t} \left(\int_{0}^{\beta} e^{-\frac{1}{\varepsilon_{i}} (\beta - \alpha)} \dot{d}_{i}^{j} \left(\alpha \right) d\alpha \right) d\beta.$$
(19)

The first term on the right-hand side of (19) is bounded by $\varepsilon_i \left| \tilde{d}_i^j (0) \right|$. The second term is equal to $\left\| h \left(t \right) * \dot{d}_i^j \left(t \right) \right\|$ where $h \left(t \right) = e^{-\frac{1}{\varepsilon_i} t}$ and * is the convolution operator. According to Young's convolution theorem [40], $\left\| h \left(t \right) * \dot{d}_i^j \left(t \right) \right\| \leq \left\| h \left(t \right) \right\| \left\| \dot{d}_i^j \left(t \right) \right\|$. Also, from the definition of \mathcal{L}_1 norm, we have $\left\| h_i \left(t \right) \right\| = \varepsilon_i$. Therefore,

$$\int_{0}^{t} \left| \tilde{d}_{i}^{j} \left(\alpha \right) \right| d\alpha \leq \varepsilon_{i} \left| \tilde{d}_{i}^{j} \left(0 \right) \right| + \varepsilon_{i} \left\| \dot{d}_{i}^{j} \right\|. \tag{20}$$

Considering that the left-hand side of (20) is the definition of \mathcal{L}_1 norm for \tilde{d}_i^j and also using (8) result in

$$\left\| \tilde{d}_{i}^{j}\left(t\right) \right\| \leq \varepsilon_{i}\left(\left| \tilde{d}_{i}^{j}\left(0\right) \right| + \delta_{i}^{j}\right),$$
 (21)

which implies

$$\left\|\tilde{\mathbf{d}}_{i}\left(t\right)\right\| \leq \varepsilon_{i}\left(\left\|\tilde{\mathbf{d}}_{i}\left(0\right)\right\| + \boldsymbol{\delta}_{i}\right).$$
 (22)

As ε_i is a small constant, (21) suggests that the disturbance estimation error is small and bounded for all time and this provides a theoretical verification for the convergence of the proposed HGDO.

IV. CONTROLLER DESIGN

Our objective in this section is to study how the proposed HGDO can be integrated into the Lyapunov-based control design. We will study SMC design here as an example and establish stability results for the HGDO and the control law.

Let us start with the definition of tracking errors. Given the desired trajectories $(\mathbf{x}_{1d}^T, \mathbf{x}_{3d}^T)^T$, we define the position tracking error as $\mathbf{e}_1 = \mathbf{x}_{1d} - \mathbf{x}_1$ and the attitude tracking error as $\mathbf{e}_2 = \mathbf{x}_{3d} - \mathbf{x}_3$. Next, we define the sliding surfaces as follows

$$\mathbf{s}_i = \dot{\mathbf{e}}_i + \lambda_i \mathbf{e}_i,\tag{23}$$

where $\lambda_i \in \mathbb{R}^3$, $i = \{1,2\}$ are design parameters with positive components. Let us now consider the following Lyapunov function candidate

$$V = \frac{1}{2} \left(\mathbf{s}_1^T \mathbf{s}_1 + \mathbf{s}_2^T \mathbf{s}_2 + \tilde{\mathbf{d}}_1^T \tilde{\mathbf{d}}_1 + \tilde{\mathbf{d}}_2^T \tilde{\mathbf{d}}_2 \right). \tag{24}$$

Taking the derivative from both sides of (24) and substituting (15) and (23) result in

$$\dot{V} = \mathbf{s}_1^T \dot{\mathbf{s}}_1 + \mathbf{s}_2^T \dot{\mathbf{s}}_2 + \tilde{\mathbf{d}}_1^T \dot{\tilde{\mathbf{d}}}_1 + \tilde{\mathbf{d}}_2^T \dot{\tilde{\mathbf{d}}}_2. \tag{25}$$

Using the tracking error definition and substituting system dynamics (6) yield

$$\dot{V} = \mathbf{s}_{1}^{T} (\ddot{\mathbf{x}}_{1d} + \mathbf{g} - \mathbf{u}_{1} - \mathbf{d}_{1} + \boldsymbol{\lambda}_{1} \dot{\mathbf{e}}_{1})
+ \mathbf{s}_{2}^{T} (\ddot{\mathbf{x}}_{3d} - \mathbf{f}_{2} (\mathbf{x}_{4}) - \mathbf{u}_{2} - \mathbf{d}_{2} + \boldsymbol{\lambda}_{2} \dot{\mathbf{e}}_{2})
+ \tilde{\mathbf{d}}_{1}^{T} \dot{\tilde{\mathbf{d}}}_{1} + \tilde{\mathbf{d}}_{2}^{T} \dot{\tilde{\mathbf{d}}}_{2}.$$
(26)

Let us define the control laws as follows

$$\begin{cases} \mathbf{u}_{1} = \ddot{\mathbf{x}}_{1d} + \mathbf{g} - \hat{\mathbf{d}}_{1} + \lambda_{1}\dot{\mathbf{e}}_{1} + \mathbf{k}_{1}\mathrm{sgn}\left(\mathbf{s}_{1}\right) + \mathbf{L}_{1}\mathbf{s}_{1}, \\ \mathbf{u}_{2} = \ddot{\mathbf{x}}_{3d} - \mathbf{f}_{2}\left(\mathbf{x}_{4}\right) - \hat{\mathbf{d}}_{2} + \lambda_{2}\dot{\mathbf{e}}_{2} + \mathbf{k}_{2}\mathrm{sgn}\left(\mathbf{s}_{2}\right) + \mathbf{L}_{2}\mathbf{s}_{2}, \end{cases}$$
(27

where $\operatorname{sgn}(\cdot)$ denotes the sign function and $\mathbf{k}_i \in \mathbb{R}^3$ and $\mathbf{L}_i \in \mathbb{R}^{3 \times 3}$ are design parameters. As it will be clarified shortly, \mathbf{L}_i must be positive-definite, and \mathbf{k}_i must satisfy a certain criterion to ensure system stability. Substituting (27) in (25) leads to

$$\dot{V} \leq -\mathbf{s}_{1}^{T}\tilde{\mathbf{d}}_{1} - \mathbf{s}_{1}^{T}\mathbf{k}_{1}\operatorname{sgn}\left(\mathbf{s}_{1}\right) - \mathbf{s}_{1}^{T}\mathbf{L}_{1}\mathbf{s}_{1}
-\mathbf{s}_{2}^{T}\tilde{\mathbf{d}}_{2} - \mathbf{s}_{2}^{T}\mathbf{k}_{2}\operatorname{sgn}\left(\mathbf{s}_{2}\right) - \mathbf{s}_{2}^{T}\mathbf{L}_{2}\mathbf{s}_{2}
+\tilde{\mathbf{d}}_{1}^{T}\dot{\tilde{\mathbf{d}}}_{1} + \tilde{\mathbf{d}}_{2}^{T}\dot{\tilde{\mathbf{d}}}_{2}.$$
(28)

For the last two terms in (28), we use (15) to write

$$\tilde{\mathbf{d}}_{1}^{T}\dot{\tilde{\mathbf{d}}}_{1} + \tilde{\mathbf{d}}_{2}^{T}\dot{\tilde{\mathbf{d}}}_{2} = -\frac{1}{\varepsilon_{1}}\tilde{\mathbf{d}}_{1}^{T}\tilde{\mathbf{d}}_{1} + \tilde{\mathbf{d}}_{1}^{T}\dot{\mathbf{d}}_{1} - \frac{1}{\varepsilon_{2}}\tilde{\mathbf{d}}_{2}^{T}\tilde{\mathbf{d}}_{2} + \tilde{\mathbf{d}}_{2}^{T}\dot{\mathbf{d}}_{2}.$$
(29)

For $\tilde{\mathbf{d}}_i^T \dot{\mathbf{d}}_i$ terms, we can use (8) and (22) to find upper bounds ρ_i as follows

$$\tilde{\mathbf{d}}_{i}^{T}\dot{\mathbf{d}}_{i} \leq \varepsilon_{i} \left(\left\| \tilde{\mathbf{d}}_{i} \left(0 \right) \right\| + \left\| \boldsymbol{\delta}_{i} \right\| \right) \left\| \boldsymbol{\delta}_{i} \right\| \leq \rho_{i}$$
 (30)

By substituting (15), (29), and (30) in (28), we get

$$\dot{V} \leq \varepsilon_{1} \|\mathbf{s}_{1}\| \left(\left\| \tilde{\mathbf{d}}_{1} \left(0 \right) \right\| + \|\boldsymbol{\delta}_{1}\| - \frac{1}{\varepsilon_{1}} \mathbf{k}_{1} \right) - \mathbf{s}_{1}^{T} \mathbf{L}_{1} \mathbf{s}_{1}
+ \varepsilon_{2} \|\mathbf{s}_{2}\| \left(\left\| \tilde{\mathbf{d}}_{2} \left(0 \right) \right\| + \|\boldsymbol{\delta}_{2}\| - \frac{1}{\varepsilon_{2}} \mathbf{k}_{2} \right) - \mathbf{s}_{2}^{T} \mathbf{L}_{2} \mathbf{s}_{2}
- \frac{1}{\varepsilon_{1}} \tilde{\mathbf{d}}_{1}^{T} \tilde{\mathbf{d}}_{1} - \frac{1}{\varepsilon_{2}} \tilde{\mathbf{d}}_{2}^{T} \tilde{\mathbf{d}}_{2} + \rho_{1} + \rho_{2}.$$
(31)

Let us now choose \mathbf{k}_i in a way that its components satisfy

$$k_i^j > \varepsilon_i \left(\left| \tilde{d}_i^j(0) \right| + \delta_i^j \right).$$
 (32)

Then, we can write

$$\dot{V} \leq -\mathbf{s}_{1}^{T} \lambda_{\max} \left(\mathbf{L}_{1} \right) \mathbf{s}_{1} - \mathbf{s}_{2}^{T} \lambda_{\max} \left(\mathbf{L}_{2} \right) \mathbf{s}_{2} \\
-\frac{1}{\varepsilon_{1}} \tilde{\mathbf{d}}_{1}^{T} \tilde{\mathbf{d}}_{1} - \frac{1}{\varepsilon_{2}} \tilde{\mathbf{d}}_{2}^{T} \tilde{\mathbf{d}}_{2} + \rho_{1} + \rho_{2},$$
(33)

where $\lambda_{max}\left(\cdot\right)$ denotes the largest eigenvalue. We can now write

$$\dot{V} \le -\kappa V + \rho,\tag{34}$$

where $\kappa = \min\left\{\lambda_{\max}\left(\mathbf{L}_1\right), \lambda_{\max}\left(\mathbf{L}_2\right), \frac{1}{\varepsilon_1}, \frac{1}{\varepsilon_2}\right\}$ and $\rho = \rho_1 + \rho_2$. Taking steps similar to (14)-(16), we get

$$V(t) \le e^{-\kappa t} V(0) + \int_0^t e^{-\kappa (t-\alpha)} \rho(\alpha) \, d\alpha, \quad (35)$$

which implies V is bounded. Subsequently, $\mathbf{s}_i\mathbf{s}$ are bounded. This means that the tracking errors are bounded. Therefore, with the control law (27) and (32), the vehicle trajectory will remain in an adjustable neighborhood of the desired trajectory.

One benefit of HGDO becomes clear in (32). Note that ε_i needs to be small to ensure fast disturbance estimation. This means that $\varepsilon_i \left(\left| \tilde{d}_i^j(0) \right| + \delta_i^j \right)$ have relatively small values, and thus, with small gains k_i^j the stability condition (32) can be satisfied. Small gains k_i^j can potentially lead to smaller control efforts.

It is worth noting that the control laws in (27) can lead to chattering due to the discontinuity of the sign function. Therefore, for practical implementations, we will replace the sign function with saturation function sat $\left(\frac{\mathbf{s}_i}{\mu}\right)$ where the slope of its linear portion is $\frac{1}{\mu}$. When $s_i^j > \mu$, the above stability results hold. Therefore, the system states will remain bounded even when the saturation function is used.

V. EXPERIMENTS

This section presents the results of our simulation and laboratory experiments to evaluate the effectiveness of the proposed HGDO-based control. Our primary focus will be on laboratory experiments. However, we will use simulations to assess the accuracy of disturbance estimations; as it is otherwise challenging due to the difficulty of measuring the exact values of disturbances in practice.

To evaluate the benefits gained by HGDO, we compare the performance of SMC+HGDO with SMC-only in the presence of disturbances. Also, where appropriate, we present results for SMC in the absence of disturbances.

The vehicle under consideration is Crazyflie 2.1 [41]. The vehicle, SMC, and HGDO parameters used throughout simulations and real experiments are given in Tab. I. For tuning the SMC parameters, we used the genetic algorithm where the objective function was the integral of squared tracking errors. Once the SMC parameters were optimized, we tuned the HGDO parameters in a quick trial-and-error process.

TABLE I: Parameter values used during experiments

Parameter	Value
a) Vehicle Parameters:	
m	28 g
J	diag $(1.4, 1.4, 2.17) \times 10^{-5} \ kgm^2$
k_T	$2.88 \times 10^{-8} \ Ns^2$
k_O	$7.24 \times 10^{-10} \ Nms^2$
l	$92 \ mm$
b) SMC Parameters:	
$oldsymbol{\lambda}_1$	$[0.3580, 0.5058, 0.3405]^T$
$oldsymbol{\lambda}_2$	$[0.3580, 0.5058, 0.3405]^T$
\mathbf{k}_1	$[-5.2608, -5.0176, -5.4351]^T$
\mathbf{k}_2	$[-8.0568, -13.6547, -1.8914]^T$
\mathbf{L}_1	diag $(-2.6304, -2.5088, -2.7176)$
\mathbf{L}_2	diag $(-4.0284, -6.8274, -0.9457)$
c) HGDO Parameters:	
$arepsilon_1$	0.05
$arepsilon_2$	0.1

A. Simulations

Figures 3 and 4 present the position and attitude tracking error of both SMC and SMC+HGDO methods in one of our simulation scenarios. The desired trajectory was a circular trajectory with a diameter of 1 m and a height of 0.5 m. For external disturbances, we used the Dryden wind turbulence model [42] for d_1 and sinusoidal disturbances for d_2 . It is evident that both methods are capable of maintaining the tracking error near zero; however, SMC+HGDO has a clear advantage throughout the mission. This stems from HGDO's capability to quickly estimate disturbances. As shown in Fig. 5, although the disturbance generated by the Dryden model is stochastic; the disturbance estimates have converged to the actual disturbance values only after a short transient time. Similar behavior is observed for the d₂ estimations (Fig. 6). Since the disturbances applied to the three axes were identical and the disturbance estimations were similar, we present the results for only one axis. To take a closer look at HGDO's transient response, we apply pulsating step disturbances to the vehicle and compare the actual disturbance values with their estimates. As depicted in Fig. 7, the disturbance estimate quickly converges to the actual disturbance value. Such a fast and accurate disturbance estimation presents a significant advantage in disturbance compensation and robust trajectory tracking, as it will be shown in the following laboratory experiments.

B. Laboratory Experiments

Scenario 1: Position-hold: In this scenario, the vehicle takes off from the origin, flies to point $(0.5, 0.5, 0.5)^T$, and hovers at this point. There is an external fan in the vicinity of the hover point generating wind disturbance. In the hover point, the vehicle resists the disturbance and holds its position. We conducted these experiments with both SMC and SMC+HGDO. We also conducted this experiment without the external fan while using SMC. Figures 8 and 9 present the vehicle trajectory and position tracking error in each trial. It is clear that, with both methods, the vehicle has successfully reached to hover point and held its position despite the disturbances. However, HGDO+SMC offers

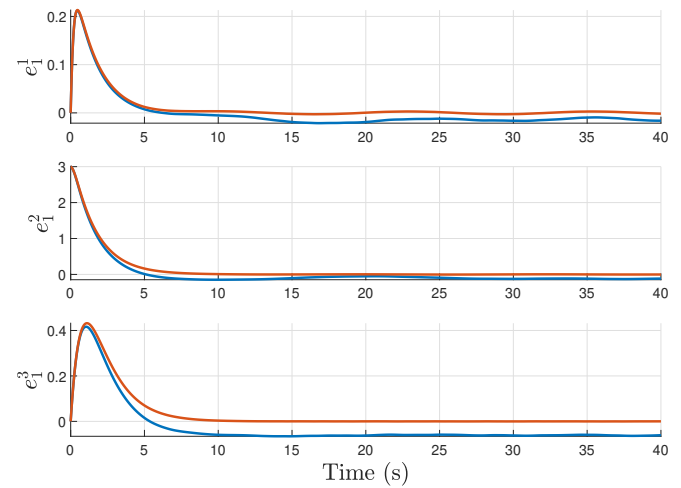


Fig. 3: Position tracking error; SMC (blue) and SMC+HGDO (coral)

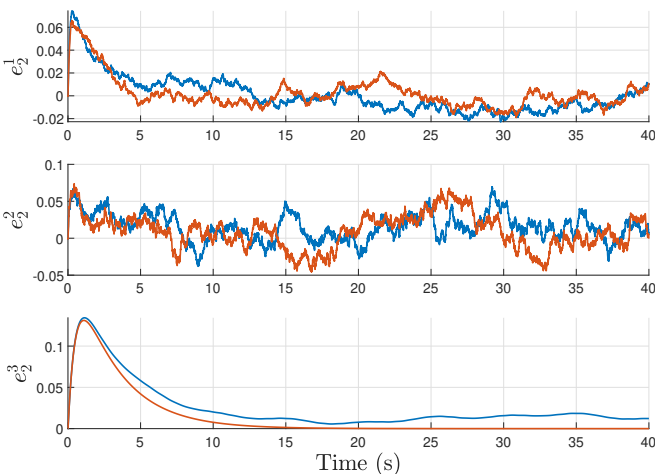


Fig. 4: Attitude tracking error; SMC (blue) and SMC+HGDO (coral)

smaller fluctuations in the hover point compared to SMC. This implies a better rejection of the constant disturbance generated by the external fan. In fact, HGDO+SMC results are comparable to SMC results in the absence of the fan. In other words, with HGDO, the vehicle can reject the effect of a constant disturbance almost entirely.

Scenario 2: Tracking a circular path: In this scenario, the vehicle tracks a circular path similar to the one mentioned in simulations. As shown in Fig. 1, an external fan generates a wind disturbance in the vicinity of the path, and the vehicle undergoes a non-uniform disturbance throughout the mission. Similar to Scenario 1, we conduct this experiment with SMC, SMC+HGDO, and SMC in the absence of disturbance. It is worth noting that in each trial, the vehicle completes the path three times. This provides a rough assessment of the precision of the methods.

The vehicle trajectory for SMC and SMC+HGDO are shown in Fig. 1. It is apparent that both the accuracy and precision of the vehicle have significantly improved with the addition of HGDO. Figure 10 takes a closer look at how the trajectory tracking error of these controllers

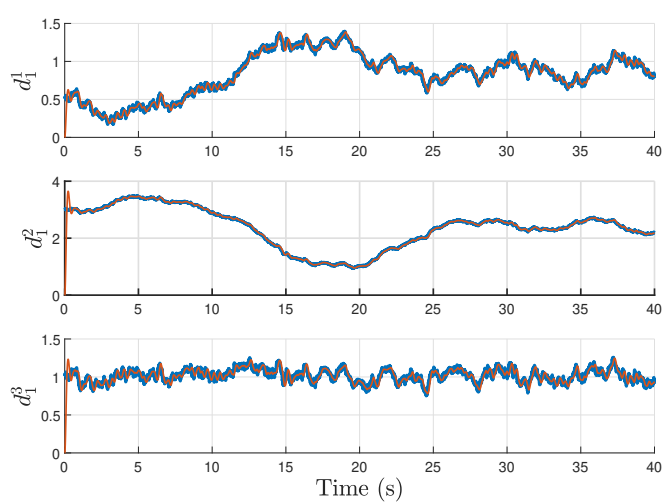


Fig. 5: Dryden wind disturbance (blue) and its estimation (coral)

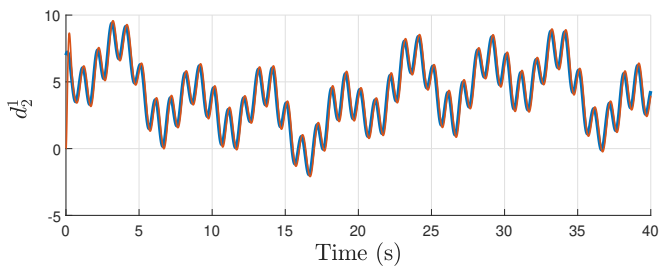


Fig. 6: One component of d₂ applied to rotational dynamics; actual disturbance (blue) and its estimation (coral)

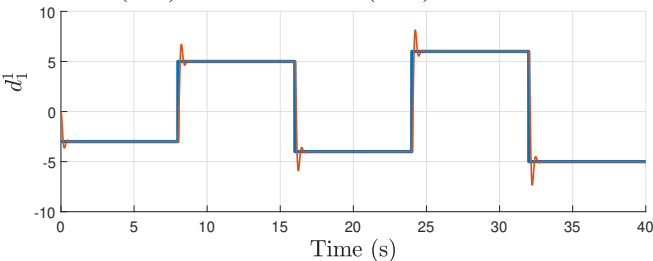


Fig. 7: One component of pulsating step disturbance applied to vehicle; actual disturbance (blue) and its estimation (coral)

are compared. The tracking error for SMC in the absence of external disturbances is also included. It is clear that with HGDO, we achieve higher accuracy even compared to SMC in the no-disturbance case. A possible explanation for this observation is that, with more aggressive maneuvers, i.e. tracking a circular path vs position hold, unmodelled dynamics in the vehicle model become significant. These unmodelled dynamics can be estimated and compensated with SMC+HGDO; thereby, resulting in a better performance compared to an SMC that relies on a simple model. The results of SMC can be potentially improved by using a more elaborated model. However, the HGDO results suggest that adding an HGDO to the control loop eliminates the need for such an elaborated model.

Scenario 3: Landing: In this scenario, the vehicle takes off from the origin, flies to point $(0.5, 0.5, 0.5)^T$ within 5 s, then returns and lands in the origin in the next 5 s. We use both SMC and SMC+HGDO methods in this scenario.

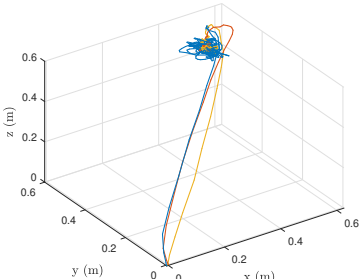


Fig. 8: Vehicle trajectory in position hold experiments; SMC (blue), SMC+HGDO (coral), and SMC in no-disturbance (yellow)

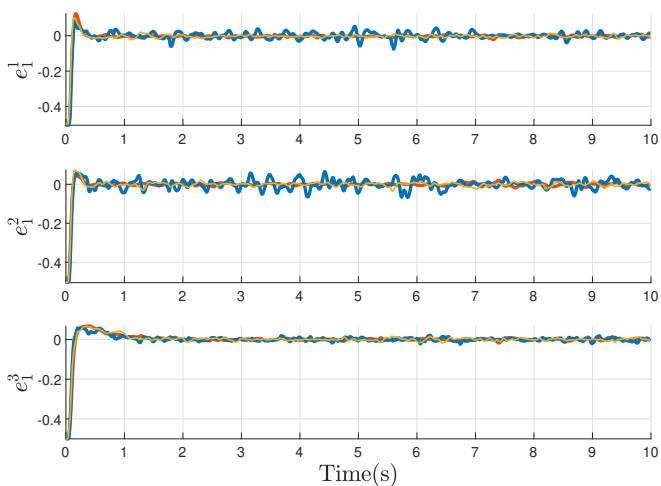


Fig. 9: Position tracking error in position hold experiments; SMC (blue), SMC+HGDO (coral), and SMC in no-disturbance (yellow)

We did not use an external fan in this case to focus on another form of external disturbance that exists due to the airflow distortion nearby the ground known as the ground effect. Figure 11 illustrates the vehicle path with both control methods. With the HGDO+SMC method, there is more consistency in the vehicle path during the departure and return phases of the mission. There exists a position error during landing; however, with SMC+HGDO, the vehicle has a considerably smaller positioning error during touchdown.

Accurate positioning during the touchdown is challenging due to the ground effect. The influence of this effect increases as the vehicle gets closer to the ground. As such, one can infer there exist larger external disturbances nearby the ground. This can be observed in the disturbance estimation plots shown in Fig. 12. Overall, due to unmodelled dynamics, there exist disturbance estimations along all axes. However, the disturbance estimate along the z-axis is relatively larger, which can be explained by the presence of the ground effect. In our landing scenario, the vehicle is close to the ground around t=0 s and t=10 s. Interestingly, \hat{d}_1^3 tends to be larger at these times suggesting that HGDO captures the ground effect. This can also explain the better positioning of the vehicle in touchdown as the ground effect is estimated and compensated by SMC+HGDO.

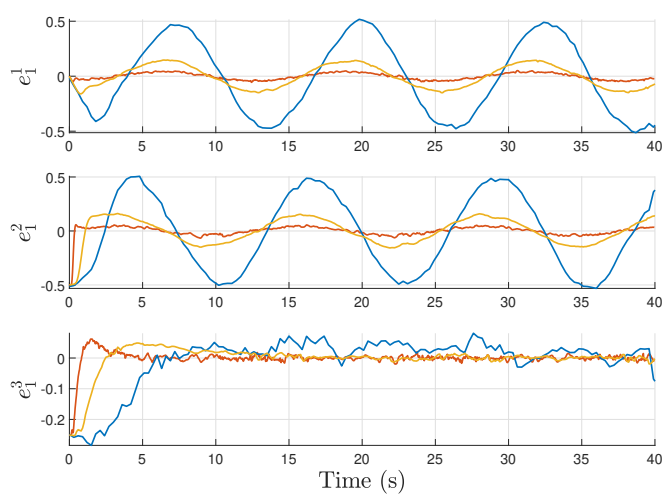


Fig. 10: Position tracking error in tracking circular path; SMC (blue), SMC+HGDO (coral), and SMC in no-disturbance (yellow)

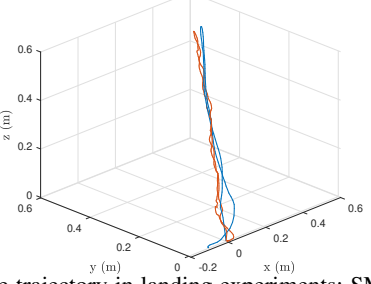


Fig. 11: Vehicle trajectory in landing experiments; SMC (blue) and SMC+HGDO (coral)

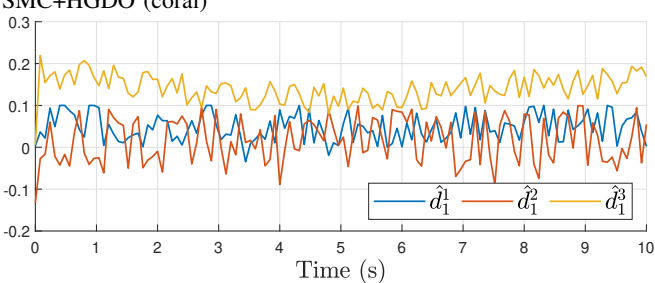


Fig. 12: Distrbance estimation in landing experiments

VI. CONCLUSION

This study developed a new HGDO for robust trajectory tracking of quadrotors. Our theoretical results established that (i) HGDO can guarantee the boundedness of disturbance estimation error with a short transient time, and (ii) HGDO combined with Lyapunov-based controllers can guarantee the boundedness of position and attitude tracking errors. Our experimental results conformed with theoretical results and demonstrated that adding HGDO to a flight controller can significantly improve the quadrotor's robustness against external disturbances. Our circular path tracking experiments revealed that HGDO can also account for unmodelled dynamics and lead to improved trajectory tracking performance compared to no-disturbance cases.

Note that despite HGDO's several desirable properties, its use in quadrotor control has remained minimal in the past. Besides the fact that the advantages of HGDO were

not thoroughly studied for quadrotors before this letter, there could be skepticism attributed to the sensitivity of conventional HGDOs to measurement noise. However, in our approach here, we still use an extended Kalman filter for state estimation, and HGDO is only an additional layer on position and attitude controllers. As a result, our HGDO-based flight control architecture was capable of handling the typical measurement noise present in inertial measurement units and motion capture systems in a common research vehicle. Therefore, we argue that HGDO is a simple, easy-to-tune, and computationally efficient module that can be added to conventional quadrotor flight control approaches to boost system robustness.

In the near future, we will explore the application of the proposed HGDO in real-world quadrotor applications that are particularly challenged by external disturbances.

REFERENCES

- [1] D. Galway *et al.*, "Modeling of the urban gust environment with application to autonomous flight," in *AIAA Atmospheric Flight Mechanics Conference and Exhibit*, 2008, p. 6565.
- [2] X. He and K. K. Leang, "Quasi-steady in-ground-effect model for single and multirotor aerial vehicles," AIAA Journal, vol. 58, no. 12, pp. 5318–5331, 2020.
- [3] J. C. Nathanael et al., "Numerical studies on modeling the near-and far-field wake vortex of a quadrotor in forward flight," Proceedings of the Institution of Mechanical Engineers, Part G: Journal of Aerospace Engineering, vol. 236, no. 6, pp. 1166–1183, 2022.
- [4] M. Greeff and A. P. Schoellig, "Flatness-based model predictive control for quadrotor trajectory tracking," in 2018 IEEE/RSJ International Conference on Intelligent Robots and Systems (IROS). IEEE, 2018, pp. 6740–6745.
- [5] K. Zhang et al., "Robust nonlinear model predictive control based visual servoing of quadrotor uavs," IEEE/ASME Transactions on Mechatronics, vol. 26, no. 2, pp. 700–708, 2021.
- [6] F. Nan et al., "Nonlinear mpc for quadrotor fault-tolerant control," IEEE Robotics and Automation Letters, vol. 7, no. 2, pp. 5047–5054, 2022.
- [7] R. Xu and U. Ozguner, "Sliding mode control of a quadrotor helicopter," in *Proceedings of the 45th IEEE Conference on Decision and Control*. IEEE, 2006, pp. 4957–4962.
- [8] Z. Hou et al., "Nonsingular terminal sliding mode control for a quadrotor uav with a total rotor failure," Aerospace Science and Technology, vol. 98, p. 105716, 2020.
- [9] E.-H. Zheng et al., "Second order sliding mode control for a quadrotor uay," ISA transactions, vol. 53, no. 4, pp. 1350–1356, 2014.
- [10] C. Nicol et al., "Robust adaptive control of a quadrotor helicopter," Mechatronics, vol. 21, no. 6, pp. 927–938, 2011.
- [11] P. De Monte and B. Lohmann, "Position trajectory tracking of a quadrotor helicopter based on 11 adaptive control," in 2013 European Control Conference (ECC). IEEE, 2013, pp. 3346–3353.
- [12] Z. T. Dydek et al., "Adaptive control of quadrotor uavs: A design trade study with flight evaluations," *IEEE Transactions on control systems* technology, vol. 21, no. 4, pp. 1400–1406, 2012.
- [13] S. Bansal et al., "Learning quadrotor dynamics using neural network for flight control," in 2016 IEEE 55th Conference on Decision and Control (CDC). IEEE, 2016, pp. 4653–4660.
- [14] P. Varshney et al., "Deepcontrol: Energy-efficient control of a quadrotor using a deep neural network," in 2019 IEEE/RSJ International Conference on Intelligent Robots and Systems (IROS). IEEE, 2019, pp. 43–50.
- [15] P. L. Donti et al., "Enforcing robust control guarantees within neural network policies," arXiv preprint arXiv:2011.08105, 2020.
- [16] J. Hwangbo et al., "Control of a quadrotor with reinforcement learning," *IEEE Robotics and Automation Letters*, vol. 2, no. 4, pp. 2096–2103, 2017.
- [17] A. Molchanov et al., "Sim-to-(multi)-real: Transfer of low-level robust control policies to multiple quadrotors," in 2019 IEEE/RSJ International Conference on Intelligent Robots and Systems (IROS). IEEE, 2019, pp. 59–66.

- [18] H. Han et al., "Cascade flight control of quadrotors based on deep reinforcement learning," *IEEE Robotics and Automation Letters*, vol. 7, no. 4, pp. 11 134–11 141, 2022.
- [19] L. Besnard et al., "Control of a quadrotor vehicle using sliding mode disturbance observer," in 2007 American Control Conference. IEEE, 2007, pp. 5230–5235.
- [20] —, "Quadrotor vehicle control via sliding mode controller driven by sliding mode disturbance observer," *Journal of the Franklin Institute*, vol. 349, no. 2, pp. 658–684, 2012.
- [21] W. Dong et al., "High-performance trajectory tracking control of a quadrotor with disturbance observer," Sensors and Actuators A: Physical, vol. 211, pp. 67–77, 2014.
- [22] M. Chen et al., "Tracking flight control of quadrotor based on disturbance observer," IEEE Transactions on Systems, Man, and Cybernetics: Systems, vol. 51, no. 3, pp. 1414–1423, 2019.
- [23] N. Ahmed et al., "Disturbance observer based tracking control of quadrotor with high-order disturbances," *IEEE access*, vol. 8, pp. 8300–8313, 2020.
- [24] A. Asignacion et al., "Frequency-based wind gust estimation for quadrotors using a nonlinear disturbance observer," *IEEE Robotics* and Automation Letters, vol. 7, no. 4, pp. 9224–9231, 2022.
- [25] W.-H. Chen et al., "Disturbance-observer-based control and related methods—an overview," *IEEE Transactions on industrial electronics*, vol. 63, no. 2, pp. 1083–1095, 2015.
- vol. 63, no. 2, pp. 1083–1095, 2015.

 [26] C. Kravaris *et al.*, "Nonlinear observer design for state and disturbance estimation," *Systems & Control Letters*, vol. 56, no. 11-12, pp. 730–735, 2007.
- [27] A. Castillo et al., "Disturbance observer-based quadrotor attitude tracking control for aggressive maneuvers," Control Engineering Practice, vol. 82, pp. 14–23, 2019.
- [28] B. Wang et al., "Disturbance observer-based adaptive fault-tolerant control for a quadrotor helicopter subject to parametric uncertainties and external disturbances," Mechanical Systems and Signal Processing, vol. 120, pp. 727–743, 2019.
- [29] H. K. Khalil, High-gain observers in nonlinear feedback control. SIAM, 2017.
- [30] N. Boizot et al., "An adaptive high-gain observer for nonlinear systems," Automatica, vol. 46, no. 9, pp. 1483–1488, 2010.
- [31] D. Won et al., "High-gain disturbance observer-based backstepping control with output tracking error constraint for electro-hydraulic systems," *IEEE Transactions on Control Systems Technology*, vol. 23, no. 2, pp. 787–795, 2015.
- [32] H. K. Khalil, "Extended high-gain observers as disturbance estimators," SICE Journal of Control, Measurement, and System Integration, vol. 10, no. 3, pp. 125–134, 2017.
- [33] C. J. Boss et al., "Uncertainty and disturbance estimation for quadrotor control using extended high-gain observers: Experimental implementation," in *Dynamic Systems and Control Conference*, vol. 58288. American Society of Mechanical Engineers, 2017, p. V002T01A003.
- [34] K. Zhao et al., "Composite disturbance rejection attitude control for quadrotor with unknown disturbance," *IEEE Transactions on Industrial Electronics*, vol. 67, no. 8, pp. 6894–6903, 2019.
- [35] Q. Lu et al., "Uncertainty and disturbance estimator-based global trajectory tracking control for a quadrotor," *IEEE/ASME Transactions* on Mechatronics, vol. 25, no. 3, pp. 1519–1530, 2020.
- [36] D. Shi et al., "Generalized extended state observer based high precision attitude control of quadrotor vehicles subject to wind disturbance," IEEE Access, vol. 6, pp. 32349–32359, 2018.
- [37] C. J. Boss and V. Srivastava, "A high-gain observer approach to robust trajectory estimation and tracking for a multi-rotor uav," arXiv preprint arXiv:2103.13429, 2021.
- [38] R. Mahony et al., "Multirotor aerial vehicles: Modeling, estimation, and control of quadrotor," *IEEE robotics & automation magazine*, vol. 19, no. 3, pp. 20–32, 2012.
- [39] S. Martini et al., "Euler-lagrange modeling and control of quadrotor uav with aerodynamic compensation," in 2022 International Conference on Unmanned Aircraft Systems (ICUAS). IEEE, 2022, pp. 369– 377
- [40] R. L. Wheeden, Measure and integral: an introduction to real analysis. CRC press, 2015, vol. 308.
- [41] Crazyflie 2.1. [Online]. Available: https://store.bitcraze.io/products/ crazyflie-2-1
- [42] T. Beal, "Digital simulation of atmospheric turbulence for dryden and von karman models," *Journal of Guidance, Control, and Dynamics*, vol. 16, no. 1, pp. 132–138, 1993.